INTERNATIONAL JOURNAL FOR NUMERICAL METHODS IN FLUIDS
Int. J. Numer. Meth. Fluids 2008; **57**:745–760
Published online 25 October 2007 in Wiley InterScience (www.interscience.wiley.com). DOI: 10.1002/fld.1641

RCM-TVD hybrid scheme for hyperbolic conservation laws

Yousef Hashem Zahran*, †

Physics and Mathematics Department, Faculty of Engineering, Port Said, Egypt

SUMMARY

We describe a hybrid method for the solution of hyperbolic conservation laws. A third-order total variation diminishing (TVD) finite difference scheme is conjugated with a random choice method (RCM) in a grid-based adaptive way. An efficient multi-resolution technique is used to detect the high gradient regions of the numerical solution in order to capture the shock with RCM while the smooth regions are computed with the more efficient TVD scheme. The hybrid scheme captures correctly the discontinuities of the solution and saves CPU time. Numerical experiments with one- and two-dimensional problems are presented. Copyright © 2007 John Wiley & Sons, Ltd.

Received 6 February 2007; Revised 10 September 2007; Accepted 11 September 2007

KEY WORDS: random choice method; Runge–Kutta methods; TVD schemes; conservation laws; Euler equations; finite difference scheme; multi-resolution; Burger equation

1. INTRODUCTION

The present work is concerned with the numerical solution of the hyperbolic conservation laws. It is well known that the exact solutions to such equations may develop discontinuities in finite time, even when the initial condition is smooth, so that one needs to consider weak solutions. A successful method should compute such discontinuities with the correct position and without spurious oscillations and yet achieve a high order of accuracy in the regions of smoothness.

Harten [1] introduced the total variation diminishing (TVD) schemes modified by many others. A third-order TVD scheme is presented in [2]. The main property of the TVD scheme is that it can be second order (or higher) and oscillations-free across discontinuities. Moreover, TVD schemes are very accurate in smooth parts. The disadvantage of the TVD schemes is that they avoid oscillations near discontinuities by locally reverting to first order of accuracy near discontinuities and extrema and are therefore unsuitable for applications involving long-time evolution of complex

*Correspondence to: Yousef Hashem Zahran, Physics and Mathematics Department, Faculty of Engineering, Port Said, Egypt.
†E-mail: yousef_hashem_zahran@yahoo.com

structures, such as in acoustic and compressible turbulence. In these applications, extrema are clipped as time evolves and numerical diffusion may become dominant.

Shock-captured methods are needed for such applications. One of these methods is the random choice method (RCM) invented by Glimm [3] and made more practical by Chorin [4]. RCM has the ability to capture discontinuities with infinite resolution (zero width). RCM uses the exact solution of the local Riemann problems (RPs) to provide numerical solutions to the general initial boundary value problem. Toro [5] presented an exact Riemann solver which was found to be more efficient than others. The RCM provides sharp discontinuities, but accuracy is poor in smooth parts of the flow.

Toro and Roe [6] introduced a hybrid scheme in which they used RCM and Roe's method and used the values of the approximate solution to switch to RCM near discontinuities.

The purpose of this paper is to combine the third-order TVD scheme [2] with RCM to produce zero width discontinuities and accurate representation of the smooth parts of the flow. RCM is used only at 'large' discontinuities and the third-order TVD scheme is used in smooth parts.

The question is how to distinguish between those regions? For this purpose, Harten [7] developed a multi-resolutions technique which is performed at every step of the temporal integration process. Here we use a more efficient multi-resolution technique presented in [8, 9]. The resulting scheme ensures that the solutions at grid points around discontinuities will always be computed by an RCM, whereas smooth tendencies will not suffer any unnecessary extra damping since they will be treated by a TVD scheme.

The rest of the paper is organized as follows. In Section 2 we review the RCM. In Section 3 we describe the third-order TVD scheme and in Section 4 a TVD Runge–Kutta method, for time integration, is presented. The multi-resolution algorithm is discussed in Section 5. In Section 6 we present the hybrid scheme. Numerical results for one-dimensional conservation laws are presented in Section 7. In Section 8 the extension to two-dimensional problems is presented. Conclusions are drawn in Section 9.

2. RANDOM CHOICE METHOD

In this section we review the RCM for one-dimensional conservation laws:

$$u_t + [f(u)]_x = 0 \tag{1}$$

along with initial and boundary conditions. Here $u(x,t)$ is the vector of unknown conservative variables and $f(u)$ is the physical flux vector. Throughout this paper, we consider only uniform grids and use the following notation: let $x_j = j\Delta x$, $x_{j\pm1/2} = x_j \pm \frac{1}{2}\Delta x$, $t^n = n\Delta t$, $u_j^n = u(x_j, t^n)$ and the cell $I_j = [x_{j-1/2}, x_{j+1/2}]$, where Δx and Δt are small spatial and time scales. Consider a control volume in x-space.

Suppose that the data at $t = t^n$ for the initial value problem (1) can be suitably approximated by a piecewise constant function over a cell of width $\Delta x = x_{j+1/2} - x_{j-1/2}$, in the form

$$u(x,t) = u_j^n, \quad x_{j-1/2} \leqslant x \leqslant x_{j+1/2} \tag{2}$$

DOI: 10.1002/fld

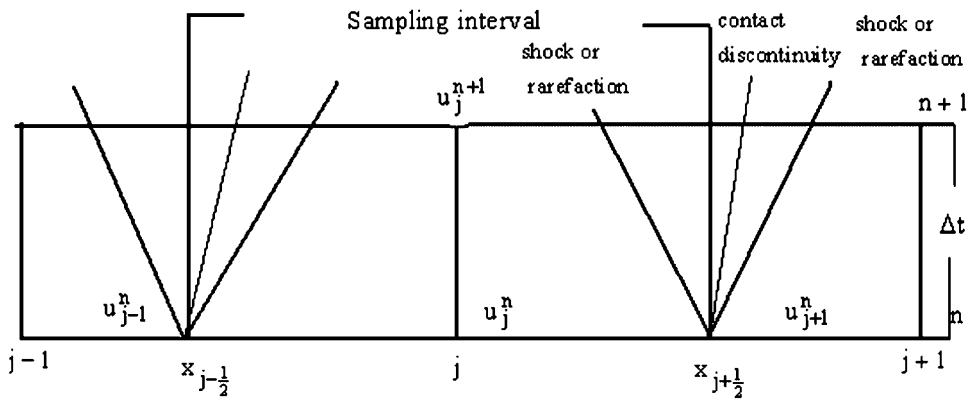

Figure 1. Solution of local Riemann problems, RP $(j-1, j)$ and RP $(j, j+1)$.

then for a sufficiently small time step Δt the original problem becomes a set of Riemann problems $\{\text{RP}(j, j+1)\}$, which is the initial value problem (1) subject to the initial condition

$$u(x, t^n) = \begin{cases} u_j^n, & x < x_{j+1/2} \\ u_{j+1}^n, & x \geqslant x_{j+1/2} \end{cases} \tag{3}$$

The exact solutions of the RPs are pieced together to form the solution of the next time level t^{n+1}. Each local problem has a solution as depicted in Figure 1 and can be solved exactly. For Euler equations efficient exact solutions are presented in [5]. The lines shown are the characteristic waves corresponding to the eigenvalues of the Jacobian matrix of $f(u)$.

Here we use the exact solution presented in [5].

Now the solution is valid locally for restricted range of space and time, i.e. before wave interaction occurs. For sufficient small Δt the local solutions are unique in their respective domains, so that the global solution at t^{n+1} is uniquely defined. RCM will take the updated solution u_j^{n+1} to be determined by the exact solution of the RP $(j-1, j)$ and RP $(j, j+1)$, evaluated at random position $Q_j = (x_{j-1/2} + \theta_n \Delta x, t^{n+1})$ in the x–t plane.

For sampling, see Figure 1. Here θ_n is a quasi-random number in the interval $[0, 1]$. For instance, if $\theta_n = 0$, then Q_j lies on the inter-cell boundary $x = x_{j-1/2}$ and the solution u_j^{n+1} is the exact solution of RP $(j-1, j)$ at that position. If $\theta_n = 1$, then Q_j is on the right inter-cell boundary at $x = x_{j+1/2}$. If $\theta_n = 0.5$, then $u_j^{n+1} = u_j^n$, i.e. the old value remains unaltered. In general, the RCM takes

$$u_j^{n+1} = V_j^{n+1}(Q_j) \tag{4}$$

where $V(x, t)$ is the exact solution of the RP.

We note that the original RCM [3] advanced the solution into two steps using a staggered grid. Here we present the one-step RCM on a non-staggered grid [5], which is simpler to implement.

DOI: 10.1002/fld

The time step size Δt is chosen to satisfy Courant–Friedrichs–Lewy (CFL) condition

$$\text{CFL} \leqslant 1$$

where $\text{CFL} = \max_j (S_j^n \Delta t / \Delta x)$. Here S_j^n is the maximum propagation speed in I_j at time level n.

3. THIRD-ORDER TVD FINITE DIFFERENCE SCHEME

In this section the third-order explicit TVD schemes presented in [2] are reviewed.

First, let us consider the linear case $f(u) = au$ in (1) so that $f'(u) = a$ is a constant wave speed.

The semi-discrete finite difference formulation of (1) in a uniformly spaced grid is

$$\frac{\mathrm{d}}{\mathrm{d}t}(u_j(t)) = \frac{-1}{\Delta x}[f_{j+1/2} - f_{j-1/2}] = L_j(u) \tag{5a}$$

where $f_{j+1/2}$ is the numerical flux.

The third-order conservative TVD numerical fluxes introduced in [2] have the form

$$\begin{aligned} f_{j+1/2} = {} & \tfrac{1}{2}(au_j + au_{j+1}) - \tfrac{1}{2}|a|\Delta_{j+1/2}u + |a|\{A_0\Delta_{j+1/2}u + A_1\Delta_{j+L+1/2}u\}\phi_j \\ & + |a|A_2\Delta_{j+M+1/2}u\phi_{j+M} \end{aligned} \tag{5b}$$

where $L = -1$, $M = 1$ for $c > 0$ and $L = 1$, $M = -1$ for $c < 0$.

Here $c = a(\Delta t/\Delta x)$ is the Courant number, and $\Delta_{j+1/2}u = u_{j+1} - u_j$, where

$$A_0 = \frac{1}{2} - \frac{|c|}{4}, \quad A_1 = -\frac{|c|}{8} - \frac{c^2}{8}, \quad A_2 = -\frac{|c|}{8} + \frac{c^2}{8} \tag{6}$$

Here ϕ_j and ϕ_{j+M} are flux limiter functions. For more details, see, [2, 10].

For nonlinear scalar problems $a = a(u)$, we define the wave speed

$$a_{j+1/2} = \begin{cases} \dfrac{\Delta_{j+1/2}f}{\Delta_{j+1/2}u}, & \Delta_{j+1/2}u \neq 0 \\ \left.\dfrac{\partial f}{\partial u}\right|_{u_j}, & \Delta_{j+1/2}u = 0 \end{cases} \tag{7}$$

The numerical flux (5a), (5b) takes the form

$$\begin{aligned} f_{j+1/2} = {} & \frac{1}{2}(f_j + f_{j+1}) - \frac{1}{2}|a_{j+1/2}|\Delta_{j+1/2}u + |a_{j+1/2}|\{A_0\Delta_{j+1/2}u + A_1\Delta_{j+L+1/2}u\}\phi_j \\ & + |a_{j+1/2}|A_2\Delta_{j+M+1/2}u\phi_{j+M} \end{aligned} \tag{8}$$

The stability condition for the above schemes is

$$\text{CFL} \leqslant 1$$

For systems of conservation laws the extension is carried out in local characteristic variables.

DOI: 10.1002/fld

4. TIME DISCRETIZATION

Up to now we have considered only spatial discretizations, leaving the time variable continuous. In this section we consider the issue of time discretization. The time discretization will be implemented by a class of high-order TVD Runge–Kutta methods developed in [11].

These Runge–Kutta methods are used to solve a system of initial value problems of ordinary differential equations (ODE) expressed as

$$\frac{\mathrm{d}u}{\mathrm{d}t} = L(u) \tag{9}$$

where $L(u)$ is an approximation to the derivative $(-f(u)_x)$ in the differential equation (1).

In [11], schemes up to third-order were found to satisfy the TVD conditions.

The optimal third-order TVD Runge–Kutta method is given by

$$\begin{aligned} u^{(1)} &= u^n + \Delta t L(u^n) \\ u^{(2)} &= \tfrac{3}{4}u^n + \tfrac{1}{4}u^{(1)} + \tfrac{1}{4}\Delta t L(u^{(1)}) \\ u^{n+1} &= \tfrac{1}{3}u^n + \tfrac{2}{3}u^{(2)} + \tfrac{2}{3}\Delta t L(u^{(2)}) \end{aligned} \tag{10}$$

In [11], it has been shown that, even with a very nice second-order TVD spatial discretization, if the time discretization is by a non-TVD but linearly stable Runge–Kutta method, the result may be oscillatory. Thus, it would always be safer to use TVD Runge–Kutta methods for hyperbolic problems.

5. MULTI-RESOLUTION ANALYSIS

The main step in the hybrid scheme proposed in this paper is how to distinguish between the smooth region and discontinuities. For this purpose, Harten [7] introduced a general framework for multi-resolution technique in order to detect the smooth and rough parts of the solution. More recently, Santos *et al*. [9] and Alves *et al*. [8] proposed a more efficient multi-resolution algorithm, called CUBISTA.

In this paper we use this algorithm to distinguish between the smooth parts and discontinuities.

Consider a set of dyadic grid of the form

$$V^j = \{x_k^j \in R:\ x_k^j = 2^{-j}k,\ k \in Z\} \tag{11}$$

where j identifies the resolution level and k the spatial location.

Assume that the function values are known on the grid V^j for $J_{\min} \leqslant j \leqslant J_{\max}$, and we want to extend it to the finer grid V^{j+1}. The even-numbered grid point function values in V^{j+1} are already present in V^j,

$$u_{2k}^{j+1} = u_k^j \tag{12}$$

The function values in the odd numbered grid points in V^{j+1} are computed using a suitable interpolation from the known even-numbered grid points (present in V^j). The normalized difference

DOI: 10.1002/fld

between the interpolated value, $I^j(u_{2k+1}^{j+1})$, and the real one, u_{2k+1}^{j+1}, is called the interpolative error coefficient (or multi-resolution coefficient), d_k^j and is expressed as i

$$d_k^j = |u_{2k+1}^{j+1} - I^j(u_{2k+1}^{j+1})|/u_{\text{ref}} \tag{13}$$

where

$$u_{\text{ref}} = \max(|u_{2i+1}^{j+1}|), \quad i = 0, 1, \ldots, 2^J$$

is a reference value of the dependent variable.

To calculate the interpolated values, we use the CUBISTA high-resolution scheme [8] as follows:

(i) Compute the face velocity

$$a_{k+1/2} = (a_k^j + a_{k+1}^j)/2$$

(ii) Compute the normalized face value $\hat{u}_{k+1/2}$, using the CUBISTA high-resolution scheme [8]; the normalized face value is given by

$$\hat{u}_{k+1/2} = \begin{cases} \max\left\{\left(\dfrac{u_k^j - u_{k-1}^j}{u_{k+1}^j - u_{k-1}^j}\right), \right. \\ \quad \left. \min\left(\dfrac{7}{4}\dfrac{u_k^j - u_{k-1}^j}{u_{k+1}^j - u_{k-1}^j}, \dfrac{3}{4}\dfrac{u_k^j - u_{k-1}^j}{u_{k+1}^j - u_{k-1}^j} + \dfrac{3}{8}, \dfrac{3}{4} + \dfrac{1}{4}\dfrac{u_k^j - u_{k-1}^j}{u_{k+1}^j - u_{k-1}^j}\right)\right\} & \text{if } a_{k+1/2} \geqslant 0 \\ \max\left\{\left(\dfrac{u_{k+1}^j - u_{k+2}^j}{u_k^j - u_{k+2}^j}\right), \right. \\ \quad \left. \min\left(\dfrac{7}{4}\dfrac{u_{k+1}^j - u_{k+2}^j}{u_k^j - u_{k+2}^j}, \dfrac{3}{4}\dfrac{u_{k+1}^j - u_{k+2}^j}{u_k^j - u_{k+2}^j} + \dfrac{3}{8}, \dfrac{3}{4} + \dfrac{1}{4}\dfrac{u_{k+1}^j - u_{k+2}^j}{u_k^j - u_{k+2}^j}\right)\right\} & \text{if } a_{k+1/2} < 0 \end{cases} \tag{14}$$

(iii) Calculate the interpolated value:

$$I^j(u_{2k+1}^{j+1}) = \begin{cases} u_{k-1}^j + \hat{u}_{k+1/2}^j(u_{k+1}^j - u_{k-1}^j) & \text{if } a_{k+1/2} \geqslant 0 \\ u_{k+2}^j + \hat{u}_{k+1/2}^j(u_k^j - u_{k+2}^j) & \text{if } a_{k+1/2} < 0 \end{cases} \tag{15}$$

The multi-resolution coefficients $\{d_k^j\}$ are used to generate a shock detection mechanism where a third-order TVD scheme is switched to an RCM whenever d_k^j is larger than a tolerance parameter ε.

The maximum and minimum level of resolution should be specified by the user to avoid coalescence in a problematic region. (Here we use $J_{\max} = 12$ and $J_{\min} = 4$.)

We must add all the grid points necessary for the calculation of the interpolative error coefficients at the next resolution level. This step is dependent on the interpolative scheme used to evaluate

DOI: 10.1002/fld

$I^j(u^{j+1}_{2k+1})$. Here we use the high resolution for which the calculation of d^j_k implies the presence of grid points at locations x^j_{k-1}, x^j_k, x^j_{k+1} and x^j_{k+2} (for more details, see, [8, 9]).

6. HYBRID METHOD

In this section, we describe the hybrid RCM-TVD scheme. It is defined as a grid-based adaptive method in which the choice of the numerical scheme is determined by the smoothness of the solution at each grid point which is measured by the multi-resolution procedure mentioned in Section 5.

The third-order TVD scheme is used at those grid points where the solution is flagged as smooth in lieu of the RCM.

The hybrid scheme is summarized in the following steps:

(1) Assume that the function values u^j_k, in the grid V^j at time $t=t_1$, compute the multi-resolution coefficients d^j_k for $J_{\min}\leqslant j\leqslant J_{\max}-1$ from Equation (13).
(2) The multi-resolution analysis is applied only once at the beginning of the Runge–Kutta time-stepping scheme. A grid point is flagged as non-smooth when $|d^j_k|>\varepsilon$ where ε is a tolerance parameter defined by the user:

$$\text{flag}_i=\begin{cases}1 & \text{if } |d_i|>\varepsilon\\ 0 & \text{otherwise}\end{cases}$$

(3) Once the flags are set, a number of neighbouring points around each flagged points x_i, depending on the number of the ghost points needed for a given difference scheme and RCM scheme, are also flagged to 1.
(4) For the grid points flagged zero (smooth), we compute u^{n+1}_j by solving the ODE (5a) using the numerical flux $f_{j+1/2}$ (5b) and the Runge–Kutta scheme.
(5) For the grid points designated as non-smooth we compute u^{n+1}_j by the RCM (4).

7. NUMERICAL RESULTS

In this section, six examples are presented to illustrate the efficiency and robustness of the proposed scheme. For all tests we use a uniform mesh; N denotes the number of cells and the exact solution is shown by the solid line and the numerical solution by symbols.

7.1. Scalar equations

We study the performance of our schemes by applying them to the following problems.

Example 1
We solve the equation

$$u_t+u_x=0,\quad x\in[-1,1] \tag{16}$$

DOI: 10.1002/fld

subjected to periodic initial data [12]

$$u(x,0)=\begin{cases}\frac{1}{6}[G(x,z-\delta)+G(x,z+\delta)+4G(x,z)], & -0.8\leqslant x\leqslant -0.6\\ 1, & -0.4\leqslant x\leqslant -0.2\\ 1-|10(x-0.1)|, & 0\leqslant x\leqslant 0.2\\ \frac{1}{6}[F(x,a-\delta)+F(x,a+\delta)+4F(x,a)], & 0.4\leqslant x\leqslant 0.6\\ 0 & \text{otherwise}\end{cases} \tag{17}$$

with periodic boundary condition on $[-1,1]$, where $G(x,z)=\exp(-\beta(x-z)^2)$, $F(x,a)=\{\max(1-\alpha^2(x-a)^2,0\}^{1/2}$.

The constants are taken as $a=0.5$, $z=-0.7$, $\delta=0.005$, $\alpha=10$ and $\beta=(\log 2)/36\delta^2$.

This initial condition consists of several shapes that are difficult for numerical methods to resolve correctly. Some of these shapes are not smooth and others are smooth but very sharp.

Here we take CFL number equal to 0.45 and $N=2^8+1$ grid points with multi-resolution tolerance $\varepsilon=10^{-3}$. Figures 2–4 show the numerical solutions at $t=20$ units obtained by the third-order TVD scheme [2], fourth-order TVD scheme [10] and the hybrid method, respectively. We observe, from the figures, that the TVD schemes produce satisfied results while the numerical solution obtained by the hybrid scheme is almost indistinguishable from the exact solution.

Example 2 (*Burgers' equation*)
This example considers the numerical solution of the inviscid Burgers' equation

$$u_t+\left(\frac{u^2}{2}\right)_x=0 \tag{18}$$

with initial condition

$$u(x,0)=\begin{cases}-1, & |x|\geqslant 0.5\\ 2, & |x|<0.5\end{cases} \tag{19}$$

The breakdown of the initial discontinuity results in a shock wave with speed 0.5 and a rarefaction with a sonic point at $x=0.5$. The exact solution consists of rarefaction wave (left) and shock wave (right). At $t=\frac{2}{3}$ the rarefaction hits the shock and then the solution has a rarefaction wave only. The numerical solution is displayed at $t=0.4$ (before collision of the head of the rarefaction with the shock) and $t=1.1$ (after collision). Results are shown in Figure 5, with 2^6+1 grid points, multi-resolution tolerance $\varepsilon=10^{-3}$ and CFL$=0.45$. Note that the hybrid method reproduces the exact solution.

Example 3 (*Two-shock Burgers' equation*)
Now we show how the hybrid method fares when the solution develops two shocks which eventually merge. We solve Burgers' equation (18) with the following initial condition [13]:

$$u(x,0)=2-\sin x+\sin 2x,\quad x\in[0,2\pi] \tag{20}$$

DOI: 10.1002/fld

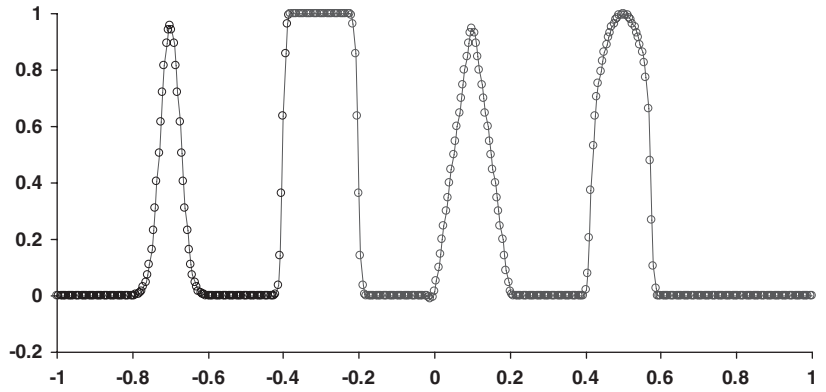

Figure 2. Solution of Example 1 using the third-order TVD scheme at $t = 20$.

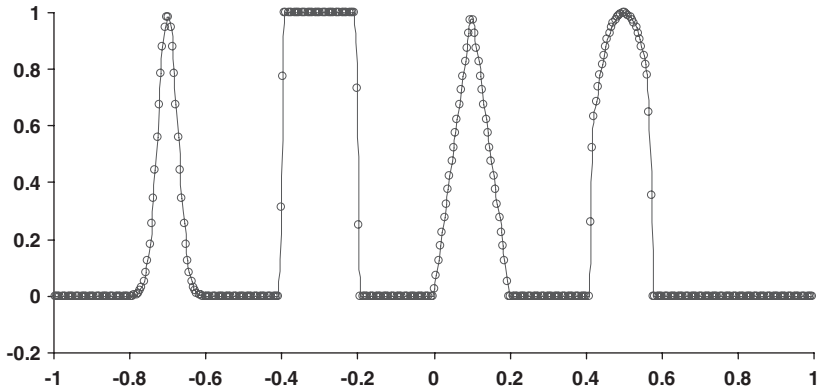

Figure 3. Solution of Example 1 using the fourth-order TVD scheme at $t = 20$.

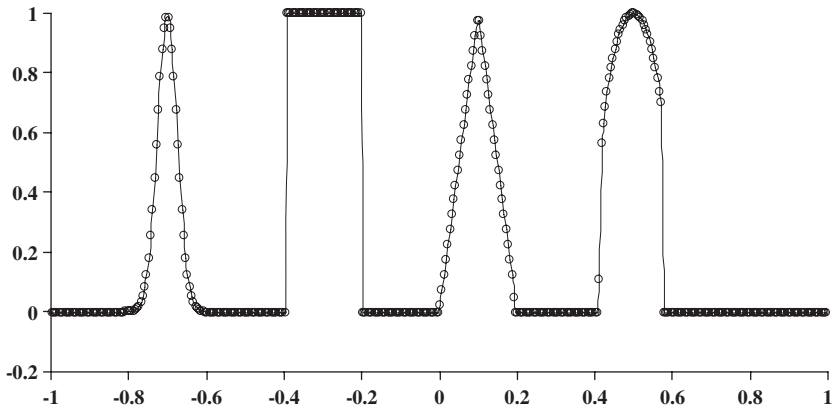

Figure 4. Solution of Example 1 using the hybrid scheme at $t = 20$.

DOI: 10.1002/fld

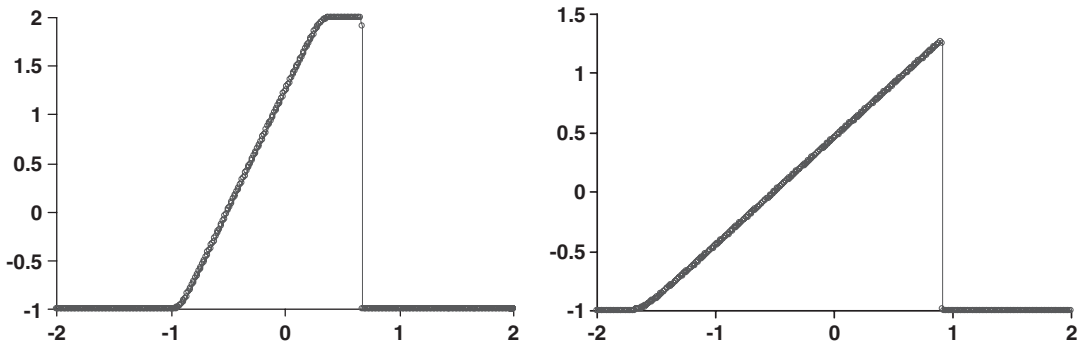

Figure 5. Solution of Example 2 using the hybrid scheme at $t=0.4$ (left) and $t=1.1$ (right).

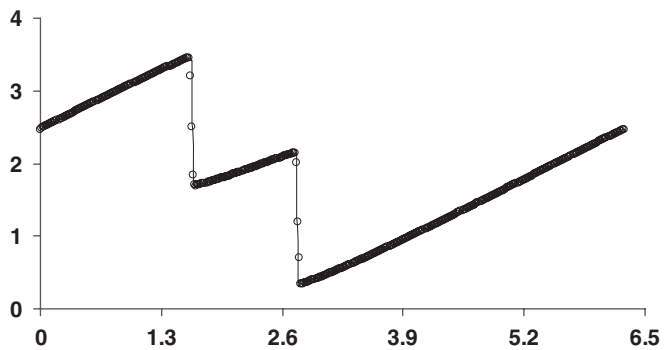

Figure 6. Solution of Example 3 using the third-order TVD scheme at $t=1.2$.

Figures 6 and 7 show the solution at $t=1.2$ obtained by third-order TVD scheme and the hybrid scheme, respectively. From the figures we note that the hybrid scheme is more efficient than the pure TVD scheme. The comparison with Figure 2 in [13] shows that the hybrid method presents the shocks correctly while the fifth-order scheme [13] presents the shocks with three points for each shock.

7.2. Systems of equations

In this section we test our hybrid scheme on the system of Euler equations of gas dynamics

$$U_t + F(U)_x = 0 \tag{21}$$

where $U=(\rho, \rho u, E)^{\mathrm{T}}$ and $F(U)=(\rho u, \rho u^2+P, u(E+P))^{\mathrm{T}}$, where ρ is the density, u is the velocity, P is the pressure, $E=0.5\rho u^2+\rho e$ is the total energy (sum of internal energy and kinetic energy); e is the specific internal energy $e=P/\rho(\gamma-1)$ and γ is the ratio of specific heats.

DOI: 10.1002/fld

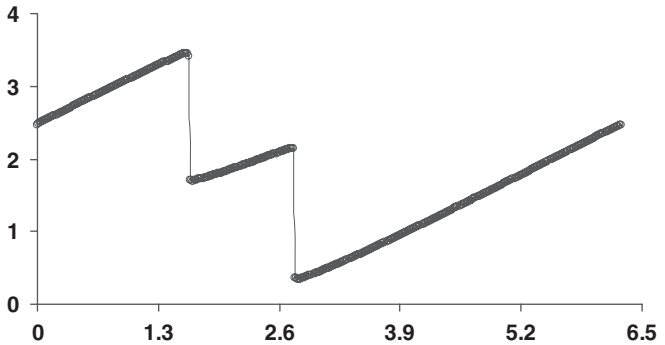

Figure 7. Solution of Example 3 using the hybrid scheme at $t=1.2$.

When performing the calculation of multi-resolution coefficient, the density field will be the one used for the analysis, since it contains not only the discontinuities due to the shocks and the rarefaction waves but also the contact discontinuities, which are present in the weak solutions of systems of conservation laws such as the Euler equations.

Example 4 (*Shock reflection problem*)
We consider the test problem concerning shock reflection in one dimension $0\leqslant x\leqslant 1$, governed by Euler equations of monatomic gas $\gamma=\frac{5}{3}$ with initial data [14]:

$$\rho=\rho_0, \quad u=u_0, \quad e=e_0$$

This represents a gas of constant density and pressure moving towards $x=0$. The boundary $x=0$ is a rigid wall and exact solution describes shock reflection from the wall. The gas is brought to rest at $x=0$ and

$$\rho_0=1, \quad u_0=1, \quad P_0=3 \tag{22}$$

$e(x,t)$ is chosen such that the pressure jump across the shock equals 2, i.e. $e_0=4.5$.

Figure 8 illustrates the results at $t=0.15$ and mesh size of 2^7+1 grid points with multi-resolution tolerance $\varepsilon=10^{-3}$ and CFL$=0.45$. We observe that the hybrid scheme resolves the discontinuity exactly.

Example 5 (*Blast wave problem*)
The blast problem introduced by Woodward and Colella [15] is a severe test problem and therefore a good problem to test the robustness of numerical schemes. This problem has the initial condition which consists of three states

$$U(x,0)=\begin{cases}(\rho_L,u_L,P_L)=(1,0,1000), & x<0.1\\ (\rho_M,u_M,P_M)=(1,0,0.01), & 0.1<x<0.9\\ (\rho_R,u_R,P_R)=(1,0,100), & x>0.9\end{cases} \tag{23}$$

DOI: 10.1002/fld

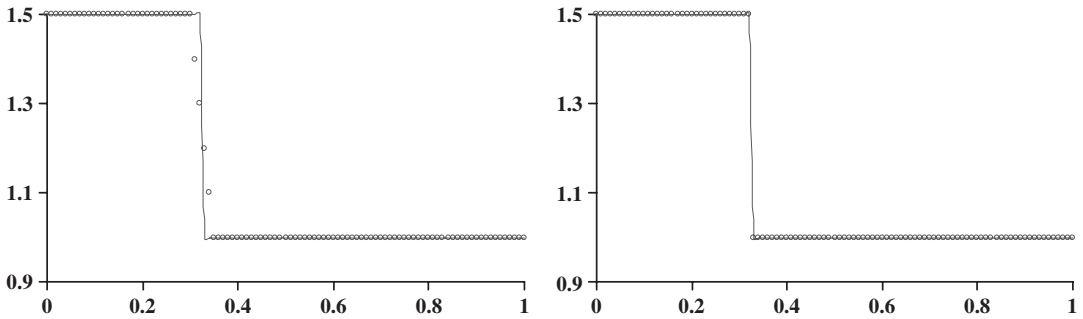

Figure 8. Solution of Example 4 using third-order scheme (left) and hybrid scheme (right) at $t=0.15$.

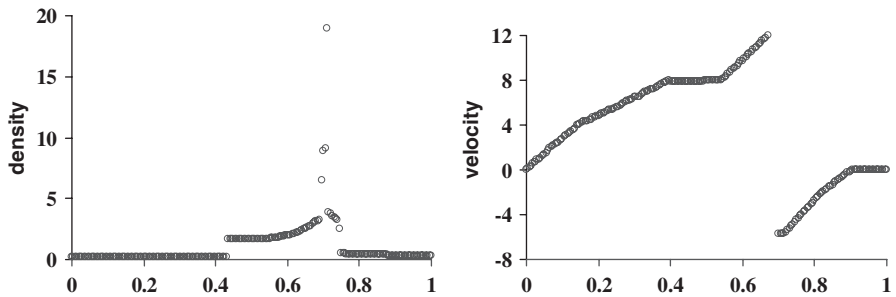

Figure 9. Solution of Example 5 using the hybrid scheme at $t=0.028$.

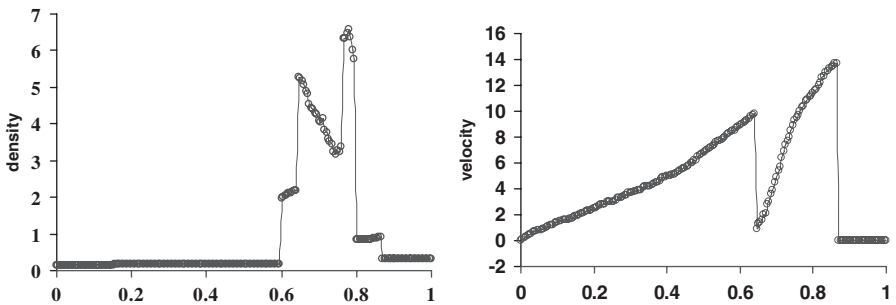

Figure 10. Solution of Example 5 using the hybrid scheme at $t=0.038$.

with $\gamma=1.4$. Boundary conditions are reflective. The solution of this problem contains the propagation of strong shock waves into low pressure regions, the collision of strong shock waves and interaction of shock waves and rarefactions, and is thus a good test of the schemes.

Figures 9 and 10 show the density and velocity obtained by the hybrid scheme at $t=0.028$ and 0.038, respectively, with 2^8+1 grid points with multi-resolution tolerance $\varepsilon=10^{-3}$ and CFL$=0.45$. It is noted that the hybrid scheme is able to obtain such sharp resolution of the complex double-blast problem, particularly, the density peaks have almost the correct value. Comparing the given

DOI: 10.1002/fld

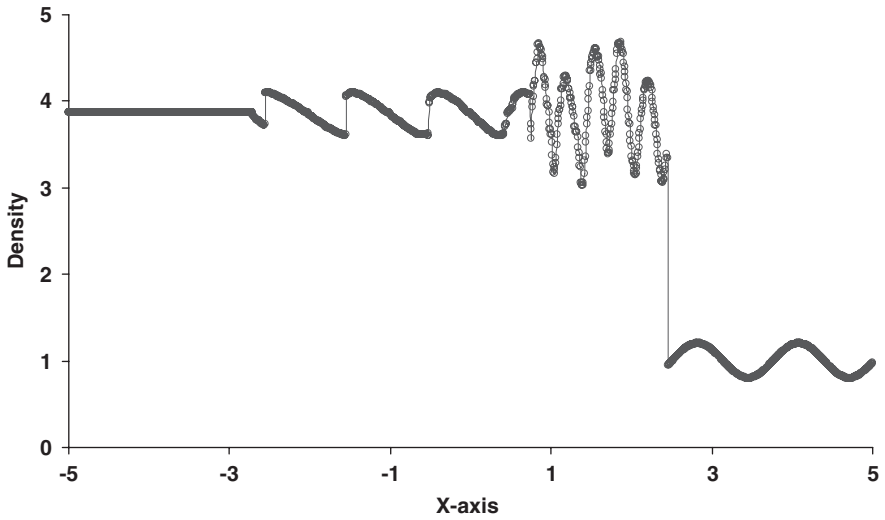

Figure 11. Solution of Example 6 using the hybrid scheme at $t=1.8$.

results with the results obtained with the reference solution shown in [15], fifth-order scheme in [13] with 400 cells and pure TVD schemes in [5] we note that our scheme is more accurate and more economical than the fifth-order scheme and TVD schemes.

Example 6 (*Shock/turbulence interaction problem*)
To show the advantages of our scheme, we will solve a problem with a rich smooth structure and a shock wave. A typical example for this is the problem of shock interaction with entropy waves [16].

We solve the Euler equations (21) with a moving Mach = 3 shock interacting with sine waves in density; i.e. initially [16]

$$\begin{aligned}(\rho_L, u_L, P_L) &= (3.857143, 2.629369, 10.3333) \quad \text{for } x<-4\\ (\rho_R, u_R, P_R) &= (1+0.2\sin 5x,\ 0,\ 1) \quad \text{for } x>-4\end{aligned} \tag{24}$$

The flow contains physical oscillations that have to be resolved by the numerical method. We compute the solution at $t=1.8$. Figure 11 shows the density computed by hybrid scheme against the reference solution, which is a converged solution computed by the fifth-order finite difference WENO scheme [16] with 2000 grid points. Here we use 2^8+1 grid points with multi-resolution tolerance $\varepsilon=10^{-3}$ and CFL$=0.45$. Comparing the results in the figure with the results shown in [13] (see Figure 4 in [13]) we observe that our scheme is more accurate than the fifth-order scheme [13] and is less expensive, because we use here 2^8+1 cells *versus* 400 cells in [13].

Remark
To show the efficiency of the hybrid scheme, we compute the CPU time for both third-order TVD and hybrid schemes as the hybrid scheme is around 30% faster than the third-order TVD scheme. This is due to the use of less-expensive RCM flux instead of TVD flux near discontinuities.

DOI: 10.1002/fld

8. EXTENSION TO MULTIDIMENSIONAL PROBLEMS

The present schemes can be applied to multidimensional problems by means of space operator splitting. As an example we consider the two-dimensional Euler equations

$$U_t + [F(U)]_x + [G(U)]_y = 0 \tag{25}$$

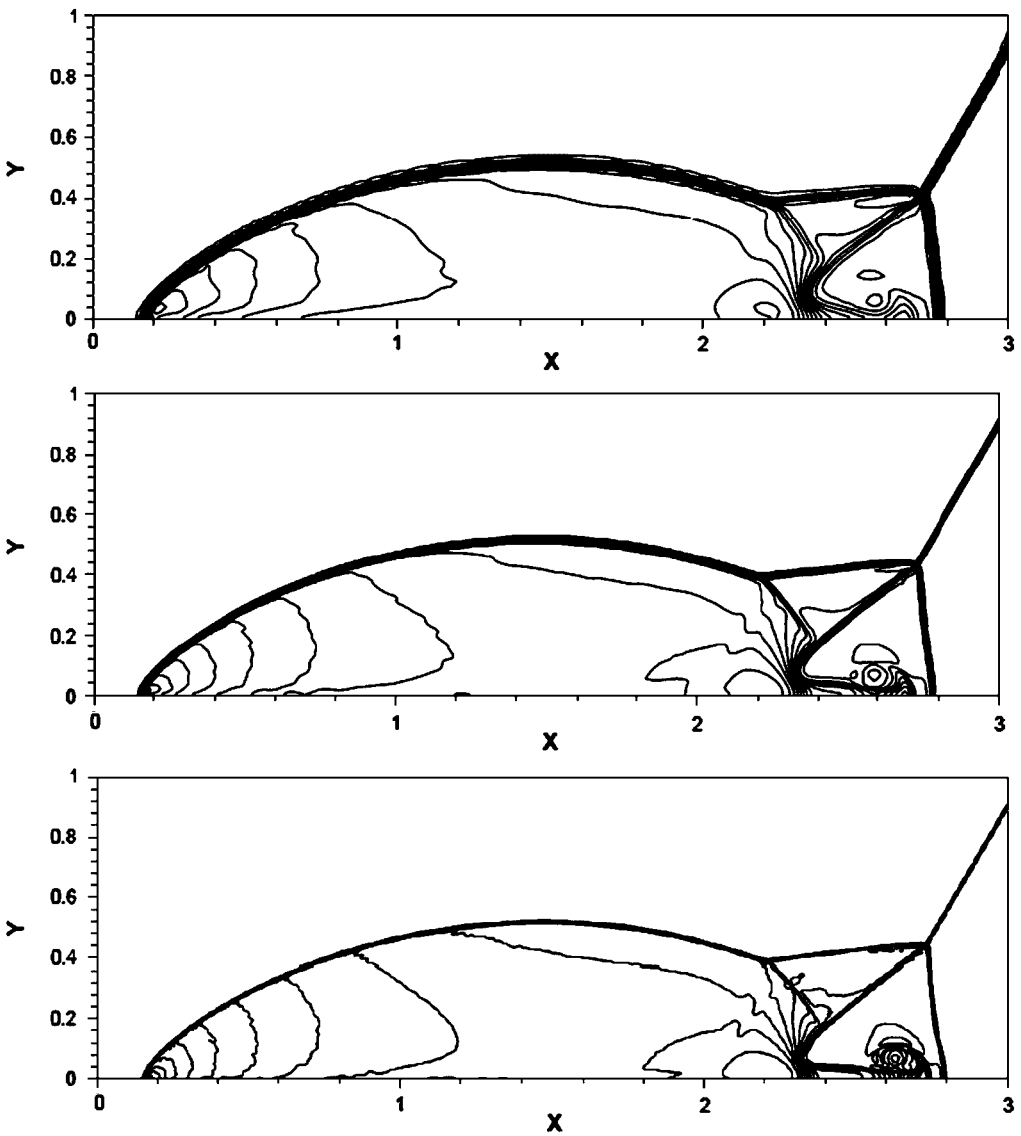

Figure 12. Double Mach refection problem for the hybrid method. Meshes of 240×60 (top), 480×120 (middle) and 960×240 (bottom).

DOI: 10.1002/fld

where $U=(\rho, \rho u, \rho v, E)^{\mathrm{T}}$, $F(U)=(\rho u, P+\rho u^2, \rho uv, u(P+E))^{\mathrm{T}}$, $G(U)=(\rho v, \rho uv, P+\rho v^2, v(P+E))^{\mathrm{T}}$.

There are several versions of space splitting. Here we take the simplest one, whereby the two-dimensional problem (25) is replaced by the sequence of two one-dimensional problems

$$U_t+[F(U)]_x=0 \tag{26a}$$

$$U_t+[G(U)]_y=0 \tag{26b}$$

If the data U^n at time level n for problem (25) are given, the solution U^{n+1} at time level $n+1$ is obtained in the following two steps:

(a) solve Equation (26a) with data U^n to obtain an intermediate solution $\overline{U}^{n+1}$ (x-sweep);
(b) solve Equation (26b) with data $\overline{U}^{n+1}$ to obtain the complete solution U^{n+1} (y-sweep).

For three-dimensional problems there is an extra z-sweep.

8.1. Double Mach reflection problem

The governing equation for this problem is the two-dimensional Euler equations (25). The computational domain is $[0, 4]\times[0, 1]$. The reflecting wall lies at the bottom of the computational domain starting from $x=\frac{1}{6}$. Initially, a right moving Mach 10 shock is positioned at $(x, y)=(\frac{1}{6}, 0)$ and makes 60° angle with the x-axis. For the bottom boundary, the exact postshock condition is imposed from $x=0$ to $x=\frac{1}{6}$ and a reflective boundary condition is used for the rest of the x-axis. At the top boundary of the computational domain, the data are set to describe the exact motion of the Mach 10 shock; refer [5] for a detailed discussion of this problem.

Figure 12 shows the computed density by hybrid scheme on the 240×60, 480×120 and 960×240 cells. We observe that the scheme produces the flow pattern generally accepted in the present literature [15] as correct. All discontinuities are well resolved and correctly positioned.

Comparing our results with those reported in [17], we observe that the accuracy of our new scheme is comparable with that of the WENO scheme [17] and superior.

9. CONCLUSIONS

We have presented an efficient, accurate and high-resolution hybrid scheme. In this scheme we use the third-order TVD scheme in the smooth region and RCM near discontinuities. The numerical solution is advanced in time by the third-order Runge–Kutta method. The main advantages of the scheme are reduction of CPU time and improvement in overall accuracy over the classical TVD schemes. This is due to the use of very cheap shock-captured RCM near discontinuities and high-order TVD scheme in the smooth region. We use an efficient multi-resolution technique to detect the discontinuities. This scheme is tested and validated by solving one- and two-dimensional problems.

REFERENCES

1. Harten A. High resolution schemes for hyperbolic conservation laws. *Journal of Computational Physics* 1983; **49**:357–393.

DOI: 10.1002/fld

2. Zahran YH. Third order TVD scheme for hyperbolic conservation laws. *Bulletin of Belgian Mathematical Society* 2007; **14**(2):259–275.
3. Glimm J. Solution in the large for nonlinear hyperbolic systems of equations. *Communications on Pure and Applied Mathematics* 1965; **18**:697–715.
4. Chorin AJ. Random choice solution of hyperbolic systems. *Journal of Computational Physics* 1976; **22**:517–536.
5. Toro EF. A fast Riemann solver with constant covolume applied to random choice method. *International Journal for Numerical Methods in Fluids* 1989; **9**:1145–1164.
6. Toro EF, Roe PL. A hybridised higher order random choice method for quasi linear hyperbolic systems. *Proceeding of the 16th International Symposium on Shock Tubes and Waves*, Aachen, Germany, 1987; 701–708.
7. Harten A. Adaptive multi-resolution schemes for shock computations. *Journal of Computational Physics* 1994; **115**:319–338.
8. Alves MA, Oliveira PJ, Pinho FT. A convergent and universally bounded interpolation scheme for the treatment of advection. *International Journal for Numerical Methods in Fluids* 2003; **41**:47–75.
9. Santos JC, Cruz P, Alves MA, Mendes A, Magalhaes FD, Pinho FT, Oliveira PJ. Adaptive multi-resolution approach for two dimensional PDEs. *Computer Methods in Applied Mechanics and Engineering* 2004; **193**: 405–425.
10. Shi J, Toro EF. Fully discrete high resolution schemes for hyperbolic conservation laws. *International Journal for Numerical Methods in Fluids* 1996; **23**:241–269.
11. Gotlieb S, Shu CW. Total variation diminishing Runge–Kutta schemes. *Mathematics of Computation* 1998; **67**:73–85.
12. Jiang GS, Shu CW. Efficient implementation of weighted ENO schemes. *Journal of Computational Physics* 1996; **126**:202–228.
13. Bryson S, Levy D. On the total variation of high-order semi-discrete central schemes for conservation laws. *Journal of Scientific Computing* 2006; **27**(1–3):163–175.
14. Glaister P. An approximate linearized Riemann solver for Euler equations for real gases. *Journal of Computational Physics* 1988; **74**:382–408.
15. Woodward P, Colella P. The numerical solution of two dimensional fluid flow with strong waves. *Journal of Computational Physics* 1984; **54**:115–173.
16. Qiu J, Shu C-W. On the construction, comparison, and local characteristic decomposition for the high order central WENO schemes. *Journal of Computational Physics* 2002; **183**:187–209.
17. Shi J, Hu C, Shu C-W. A technique for treating negative weights in WENO schemes. *Journal of Computational Physics* 2002; **175**:108–127.

DOI: 10.1002/fld